Temperature Elevation in the Human Eye Due To Intraocular Projection Prosthesis Device

Dipika Gongal
Department of Civil and Materials Engineering,
University of Illinois at Chicago,
Chicago, IL 60607
e-mail: dgonga2@uic.edu

Siddhant Thakur
Surgical Planner II, Arthrex Inc.,
Naples, FL 34119
e-mail: siddhant.thakur@arthrex.com

Ashay Panse
Department of Civil and Materials Engineering,
University of Illinois at Chicago,
Chicago, IL 60607
e-mail: apanse2@uic.edu

John A. Stark
Department of Civil and Materials Engineering,
University of Illinois at Chicago,
Chicago, IL 60607
e-mail: jstark24@uic.edu

Charles Q. Yu
Department of Ophthalmology, Byers Eye Institute,
Stanford University,
Palo Alto, CA
e-mail: chyu83@stanford.edu

Craig D. Foster[1]
Associate Professor
Computational Mechanics Laboratory,
Department of Civil and Materials Engineering,
University of Illinois at Chicago,
Chicago, IL 60607
e-mail: fosterc@uic.edu

Corneal opacity is a leading cause of blindness worldwide. Corneal transplantation and keratoprosthesis can restore vision but have limitations due to the shortage of donor corneas and complications due to infection. A proposed alternative treatment using an intraocular projection prosthesis device can treat corneal disease. In this study, we perform a transient thermal analysis of the bionic eye model to determine the power the device can produce without elevating the eye tissue temperature above the 2°C limit imposed by the international standard for implantable devices. A 3D finite element model, including blood perfusion and natural convection fluid flow of the eye, was created. The device was placed 1.95 mm from the iris, which experienced less than 2°C rise in the tissue temperature at a maximum power dissipation of LED at 100 mW and microdisplay at 25 mW. [DOI: 10.1115/1.4050237]

Keywords: thermal eye model, finite element analysis, corneal prosthesis, natural convection, bioheat transfer

1 Introduction

In a healthy eye, light enters through the cornea, and the lens focuses the light on the retina to form an image. However, for patients who suffer from corneal opacity, light cannot pass through the diseased cornea; hence, causing vision loss. A corneal transplant can restore vision, but for severe cases of opacity, the treatment is ineffective [1]. Moreover, a shortage of donor corneas persists, with 12.7 million people on a waitlist for the surgery [2]. Another treatment option is keratoprosthesis, which involves replacing the diseased cornea with an artificial one. The cornea transplants are sometimes effective, but are easily infected and can have other complications [3].

A bionic eye implant [3,4] is a potential alternative to restore sight for the patients. The implant consists of a projector that is placed on the anterior part of the eye. It receives image data wirelessly from an externally mounted camera and projects the image on the retina. The device bypasses the diseased cornea and makes vision possible.

The proposed intraocular projection device consists of LED, reflector, microdisplay, thermal adhesive, and lens enclosed in a housing (Fig. 1). The device operates with microdisplay at a power of 25 mW, while the LED power can be adjusted from 25 mW to 100 mW. The image's quality formed on the retina improves with the power dissipation by the device. However, electronic devices that operate at high power dissipate a large amount of heat to the surrounding fluid and tissue, causing temperature increase in the eye [5]. To safeguard the living tissues from exposure to high temperature, the Active Implantable Medical device (AIMD, ISO 14708-1:2014) has imposed a guideline to restrict the temperature increase to no more than 2°C above the body temperature [6]. Thus, a power budget must be established for the device.

Several studies have been performed to determine the thermal increase in the eye by a bioimplant's operation. Piyathaisere et al. [7] measured the temperature increase in the eye due to an intraocular heater device. The study was performed to identify thermal parameters to develop an implantable intraocular electronic retinal prosthesis. DeMarco et al. [8] developed a two-dimensional model of the human eye and head to study the thermal response of an implanted retinal prosthesis. Gosalia et al. [9] used an explicit finite-difference time-domain method to analyze the thermal effect on the eye by retinal prosthesis device. Their study demonstrated that temperature increase in the tissue depends upon the location and size of the implant. Lazzi [5] showed that the power dissipation by the implantable device affects the temperature increase in the eye tissue. Opie et al. [10,11] used a 3D thermal finite element model of a cat eye to determine the retinal tissue temperature increases due to a retina implant and determined the power budget of the device. All these studies on the thermal modeling for eye have focused on retina implants closer to the back of the eye and not implants for corneal blindness located at the anterior part of the eye.

A preliminary steady-state thermal analysis was performed to study the thermal response of the proposed intraocular device

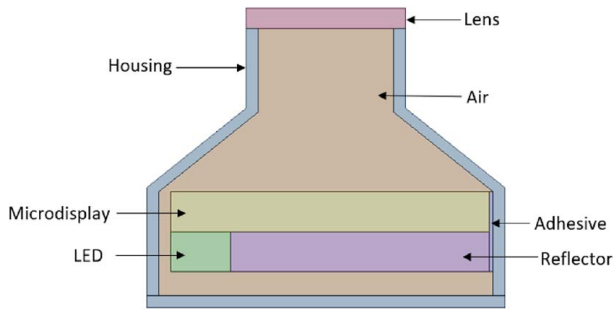

Fig. 1 Sectional view of the proposed intraocular projection device model

[1]Corresponding author.

Manuscript received September 26, 2020; final manuscript received January 24, 2021; published online April 19, 2021. Assoc. Editor: Rui Qiao.

using a two-dimensional axisymmetric model [12]. The study was followed by a three-dimensional steady-state thermal finite element analysis to establish the device's threshold of power dissipation [13]. The simulation result showed that the device is compliant with the international standard up to the LED power of 82 mW when placed 9.98 mm from the retina. The device was modified by extending the air gap between the reflector and housing by 0.5 mm to satisfy the temperature limit for the maximum LED power of 100 mW. The study included conduction, convection, radiation, and evaporation mode of heat transfer only. The blood perfusion in the eye and heat convection flow in the eye's fluid were not taken into consideration.

The blood flows in the choroid, retina, ciliary muscle, and iris tissues, while the remaining tissues are avascular [14]. The blood flow affects the eye's temperature distribution and is the primary mechanism for cooling the posterior region of the eye [15]. Previous studies that analyzed the temperature increase induced by prosthetic implants [5,8,9,11], laser radiation [16,17], and thermal therapy [18,19] considered cooling of the retina tissue due to blood perfusion. Including this parameter to our previous model can improve the accuracy of the eye's thermal elevation prediction.

Similarly, the natural convection flow of the aqueous humor contributes to the heat transfer in the eye [20,21]. The aqueous humor flows under normal conditions, and a temperature difference as low as 0.02°C can initiate flow in the fluid [22,23]. The vitreous humor, on the other hand, is stagnant under normal conditions. During the intraocular projection device implant surgery, the vitreous humor is replaced by saline solution. Saline solution however has a viscosity similar to that of aqueous humor and will experience natural convection flow.

The objective of this study is to develop a thermal model of the human eye, considering choroidal blood perfusion and natural convection thermal flow of saline solution to accurately represent the human eye. The influence of the additional thermal factors on the temperature elevation in the ocular tissue will be investigated, and the power budget of the projection device will be established.

2 Finite Element Model

2.1 Bionic Eye Geometry Model. A human ocular globe model was developed based on the data provided by the US Army Research Laboratory [24] and Atlas of the Human Eye [25]. The shape and dimensions of the iris were based on the measurements by Li and Huang [26]. The three-dimensional geometric model was created in CREO PARAMETRIC 5.0. The model was measured 24.79 mm along the anterior and posterior direction and 24 mm along the transverse and vertical direction.

A separate model of the intraocular projection device was created. It measures 9 mm × 7 mm at the back and is 7.5 mm front to back (Fig. 1). The details of the projector parts are given in Table 1.

During a bioimplant eye surgery, the lens and zonule fibers are removed and replaced by the intraocular device. The vitreous humor is drained and replaced with a saline solution. The eye model was modified accordingly to replicate the bionic eye. The projector model was placed 9.98 mm measured from the lens to the retina along the optical axis. The minimum distance between the iris and the projector was measured to be 1.95 mm. The projector was centrally placed by coinciding with the mid planes of the eye and the projector models. In the absence of the lens, the anterior chamber and posterior chamber combine to become a single chamber. So, the aqueous humor and vitreous humor parts were merged together to create a single homogeneous fluid body of saline solution. This model is the original model or Model 1 of our previous analysis [13]. Figure 2 shows the model used for the analysis.

Table 1 Components of the intraocular projection device

Parts	Dimension (mm)	Material
LED	2 × 1.5 × 1	ABS Plastic
Microdisplay	8 × 6 × 1	Glass
Reflector	6.5 × 6 × 1	ABS Plastic
Lens	4 diameter × 0.5	Glass
Thermal adhesive	6 × 2 × 0.1	Adhesive
Housing	0.3 thick	PMMA

The symmetry of the finite element model along the sagittal plane was utilized, and half of the model was used for the transient thermal analysis. The model was discretized with a combination of hexahedral and tetrahedral elements as shown in Fig. 3. A convergence test was carried out to determine the solution independent of the mesh size using the maximum temperature in the iris as the benchmark. Results from the test are tabulated in Table 2. A total number of 894,095 elements was finalized for meshing the model.

2.2 Thermal Model and Boundary Conditions. The blood flow in the eye helps to regulate the eye tissue temperature [11]. It acts as a heat sink by dissipating the heat away from the eye or serves as a heat source when eye temperature drops below the body temperature. Lagendijk [27] used the heat transfer coefficient between the sclera and the body to account for blood flow in the retina and the choroid regions. A similar approach was used by Scott [15,28] to study the temperature rise in the human eye when exposed to infrared radiation. Such a simplified heat transfer ignores the blood flow in the iris region of the eye. Flyckt et al. [29]

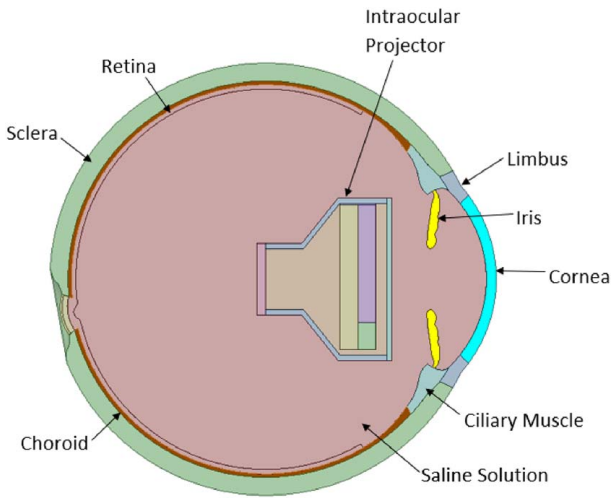

Fig. 2 The eye model with the intraocular projection device implanted after removing the lens and zonules fibers, and aqueous humor replacing the saline solution

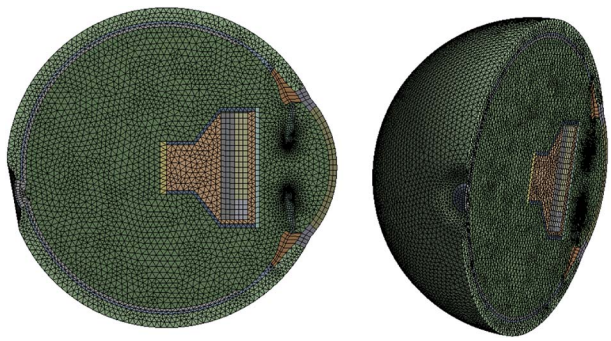

Fig. 3 Two views of the meshed model of the bionic eye

Table 2 Result of convergence study

No. of elements	Maximum Iris temperature (°C)
120,678	38.76793
450,746	38.69078
758,323	38.66265
894,095	38.64431

showed that the heat transfer coefficient found by the Lagendijk method underestimates the blood flow in the eye by comparing the temperature distribution in the eye with the models using the Pennes bioheat equation and a model with discrete blood vessels. Ng and Ooi [30], Ooi et al. [20], and Tiang and Ooi [21] used bioheat analysis for the thermal simulation. However, the blood perfusion term and the metabolic heat generation term were neglected. Narasimhan and Sundarraj [19] used the Pennes bioheat equation to create the thermal model of the human eye by taking the separate value of blood perfusion and metabolic heat generation for the choroid, retina, iris, and ciliary tissues. Shafahi and Vafai [31] introduced a modified Pennes bioheat equation with iris/sclera modeled as a porous medium to analyze the eye's thermal characteristics during exposure to thermal disturbances. Gosalia et al. [9], Lazzi [5], and Opie et al. [11] used temperature-dependent metabolic and blood perfusion rate for the choroid and retina tissue to determine the thermal effects of bioimplant.

The Pennes bioheat equation considers thermal mechanisms like heat conduction, blood perfusion, and metabolic heat generation or external heat source. It is expressed in Eq. (1)

$$\rho c \frac{\partial T}{\partial t} = \nabla \cdot k \nabla T + \omega_b \rho_b c_b (T_b - T) + Q \tag{1}$$

In this equation, ρ is the density, c is the specific heat, k is the thermal conductivity of eye tissue, T_b is the blood temperature, ω_b is the volumetric blood perfusion rate per unit volume, ρ_b is the density of the blood, c_b is the specific heat capacity of the blood, and Q is the metabolic heat generation. The value of blood temperature (T_b) is taken as 37°C, blood density (ρ_b) as 1050 kg/m^3 and, specific heat capacity (c_b) is taken as 3600 J/kg C [29].

The flow of the aqueous humor is buoyancy-driven as shown by Kumar et al. [23]. They created a three-dimensional model of the anterior chamber of the eye to study the different flow patterns of the fluid with respect to the orientation of the eye. They performed steady-state analysis and used Boussinesq approximation for the density. Ooi et al. [20] performed a two-dimensional transient thermal analysis of the human eye to study the flow of aqueous humor in the anterior chamber under the presence of an artificial heat source inside the eye. Tiang and Ooi [21] used a three-dimensional model of the eye to demonstrate that aqueous humor flow contributes to almost 95% of the total heat flow in the anterior chamber when exposed to an external heat source. For this device, the vitreous humor is also replaced with a saline solution, making the impact of convection even higher than in previous researches.

Previous published works have used Boussinesq approximation [18–23,31,32] to simulate the buoyancy-driven flow. However, with the saline solution replacing the vitreous humor, a more accurate model was needed for convection for this device. Hence, a full transient simulation was performed until the temperature reached a steady-state. Moreover, the density of the saline solution with respect to the temperature is non-linear, and the temperature difference in the domain is not small, so a transient study was performed in this research. The saline solution's density was provided as a piecewise linear function of temperature. The viscosity of the saline solution was taken as 0.000711 kg/m-s [33–35], and the operating pressure was assumed to be equal to the intraocular pressure of 15 mm Hg. Gravitation acceleration of −9.81 m/s^2 was provided in the vertical direction to create a buoyancy-driven flow.

Table 4 Material properties of the intraocular device components

Parts	Density, ρ, kg/m^3	Thermal conductivity, k, W/mC	Specific heat, c, J/kg C
PMMA [36]	1200	0.25	1466
ABS Plastic [37]	1050	0.21	1720
Adhesive [38]	1470	1.85	300
Glass [39]	2500	0.8	800

The thermal properties for each region of the eyes that are available in the literature are given in Table 3. Each region is assumed to be homogeneous and thermally isotropic. The properties of the limbus and optical nerve head were not available in the literature. Thus, they were assumed to be equal to that of the sclera tissue. The thermal properties of the projector components are given in Table 4.

The boundary conditions for the analysis were kept identical to the previous study [13]. The ambient temperature was assumed to be 40°C to represent the extreme case. Heat transfer from the cornea and limbus surface to the surrounding environment occurs through convection, evaporation, and radiation [15]. The value for the heat transfer coefficient was taken as 10 W/m^{2}K, and the evaporation rate was taken as 40 W/m^2. Radiation heat transfer was based on Stefan–Boltzmann constant value of 5.67×10^{-8} W/m^{2}K^4 and the emissivity value of 0.975. On the sclera surface, convection boundary condition was applied with the heat transfer coefficient value of 65W/m^{2}K while the temperature boundary condition of 37°C was also applied.

The projector was set to operate at the maximum power of LED at 100 mW, and the microdisplay at 25 mW to evaluate the maximum temperature elevation in the eye.

3 Results and Discussion

Transient thermal analysis of the eye model was performed using Fluent (V 19.2). The problem was initiated at 37°C for the entire model. The analysis was allowed to run until the temperature in the eye tissues became constant with respect to flow time, that is the steady-state was achieved. The results presented here are reported at the steady-state condition. The resulting temperature

Table 3 Material properties of eye tissues

Parts	Density ρ, kg/m^3	Thermal conductivity k, W/mC	Specific heat c, J/kg C	Blood perfusion rate, ω_b, 1/s	Metabolic Heat, Q, W/m^3
Cornea	1050 [18]	0.580 [18]	4178 [18]	0 [16]	0 [16]
Sclera	1050 [18]	1.0042 [18]	3180 [18]	0 [16]	0 [16]
Iris	1050 [18]	1.0042 [18]	3180 [18]	0.004 [18]	690 [16]
Choroid	1050 [11]	0.600 [11]	4178 [11]	0.021 [16]	1000 [16]
Retina	1039 [11]	0.565 [11]	3680 [11]	0.035 [16]	10000 [16]
Cilliary muscle	1040 [5]	0.498 [5]	3430 [5]	0	0
Saline solution	999.97 [33,34]	0.626 [33,34]	4130 [33,34]	–	–

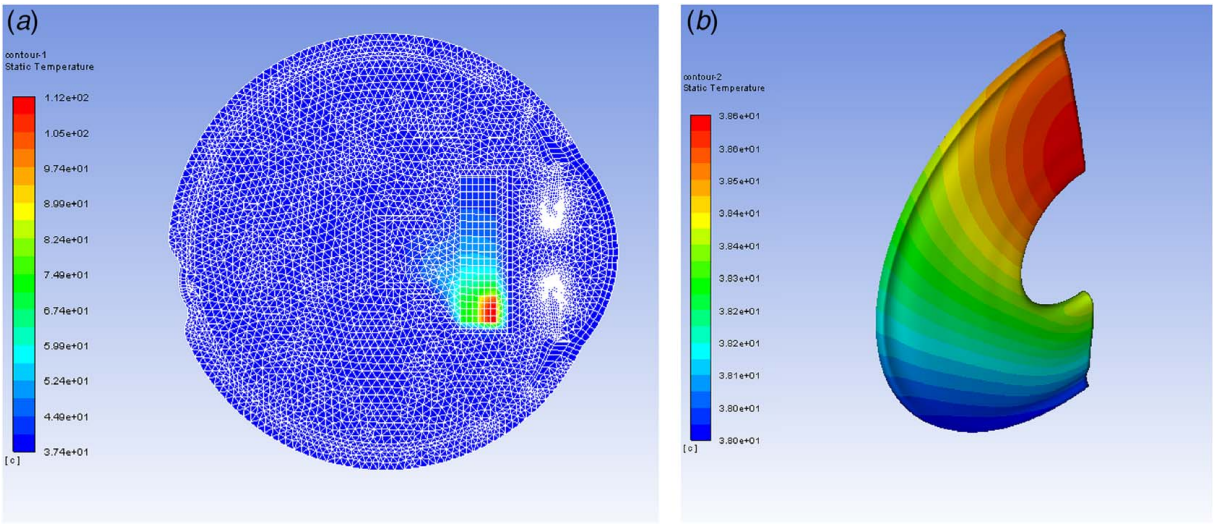

Fig. 4 (*a*) Temperature distribution contour of the eye implanted with an intraocular projecting device with LED operating at 100 mW. (*b*) Temperature contour of the iris tissue experienced the maximum temperature elevation due to the operating intraocular device.

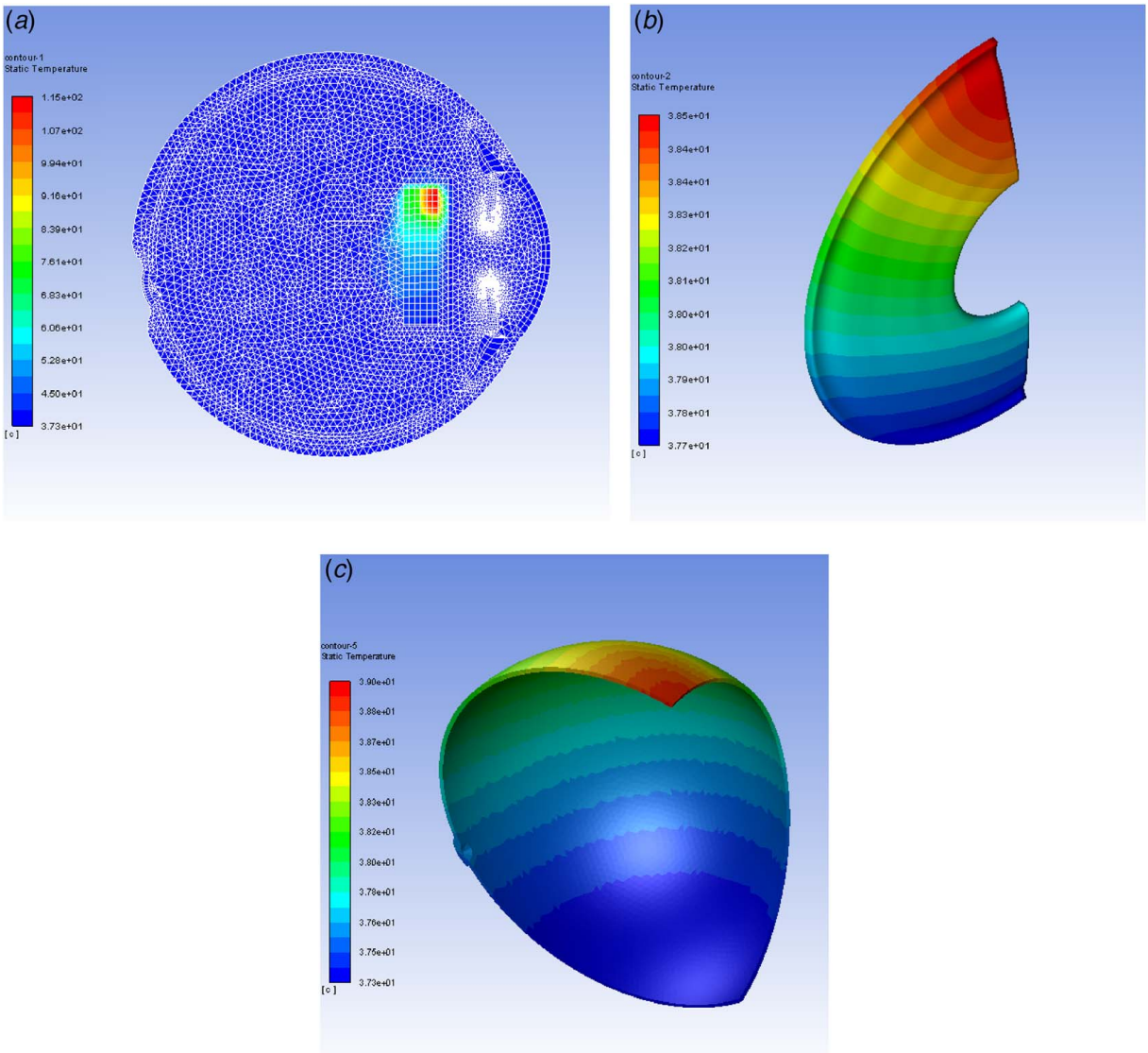

Fig. 5 Temperature distribution contour of (*a*) eye, (*b*) iris, and (*c*) retina with LED positioned at the top

Table 5 Maximum iris temperature values for LED operating at 100 mW power and projector placed at 1.95 mm away from the iris

	Previous analysis result [13]	LED at the bottom	LED at the Top
Maximum iris temperature (°C)	39.36	38.64	38.50

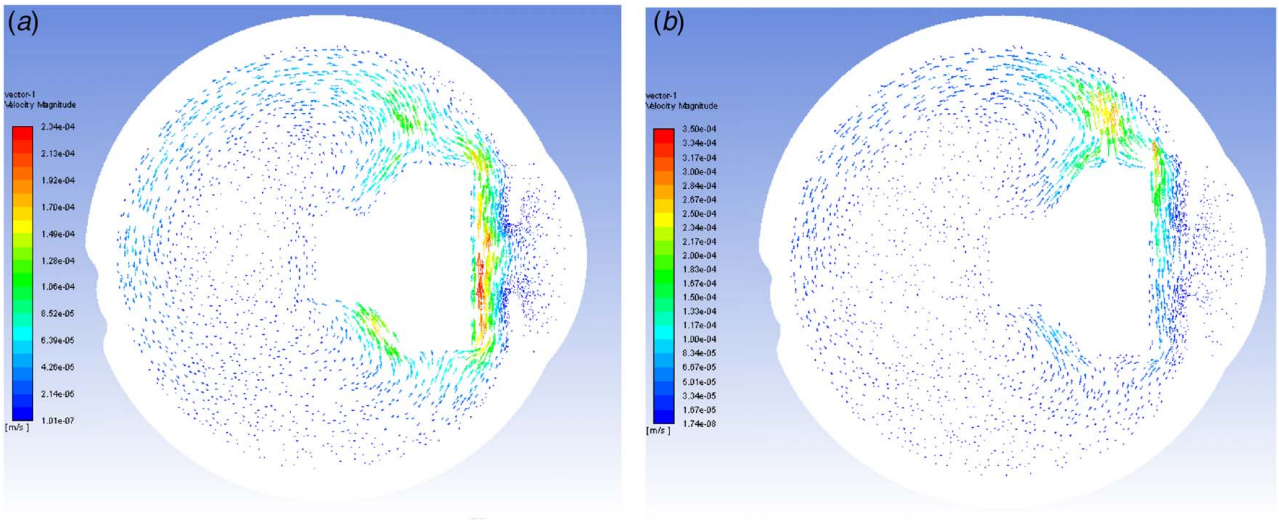

Fig. 6 Velocity vector of natural convection flow in saline solution induced by heat generated in the LED positioned at (*a*) top and (*b*) bottom

distribution in the eye with LED power dissipation set at 100 mW is presented in Fig. 4. The maximum temperature in the iris, the nearest living eye tissue, was found to be 38.64°C. The temperature increase satisfied the 2°C limit imposed by the international standard.

The model created for the analysis has the LED positioned at the bottom of the eye. In real implant surgery, it may be positioned at different locations. To investigate its impact, a second model was created with LED at the top location. The resulting maximum temperature in the iris was only 38.50°C. The maximum increase in temperature for this case was observed in the retina tissue at 38.99°C. Figure 5 shows the temperature contour plot of the eye, and the iris with the LED is at the top position.

When comparing the maximum temperature in the iris tissue with the result from the previous study [13] that did not include convection and blood perfusion, the temperature decreased by 0.72°C. The comparative result is shown in Table 5. It was observed that the flow of the saline solution circulated upward and transferred the heat toward the posterior part of the eye, as shown in Fig. 6. The saline flow interferes with thermal transfer from the projector to the iris and prevents the iris temperature from elevating significantly. When LED is at the bottom, the maximum temperature in the iris is at the top part of the iris. For the case when LED was placed at the top, the heat circulates to the posterior part of the eye, decreasing the iris temperature but elevating the temperature of the retina and limbus at 38.99°C and 38.69°C, respectively.

4 Conclusions

In this study, we performed a thermal analysis of an eye model implanted with an intraocular projection device. The analysis included blood perfusion and the natural convection flow of the saline solution. It was observed that the maximum iris temperature decreased when the effects of perfusion and natural convection flow were considered, confirming that they help to dissipate heat.

The positioning of the LED showed a significant influence on the temperature elevation in the eye tissue. The flow of the saline in the upward direction increased the tissue temperature above the LED. When LED was placed on the bottom, the temperature elevated at the top of the iris tissue. Similarly, when the LED was placed on the top, the maximum temperature increase occurred in the retina tissue.

The study showed that the projection device can operate safely with the LED power dissipation at 100 mW without increasing the tissue temperature by more than 2°C. Thus, establishing the power budget of the device at its maximum capacity. However, it must be noted that the minimum distance between the iris and the projector should be maintained at 1.95 mm to maintain a reasonable margin of safety. If this distance cannot be maintained, some modification to the projector may be necessary, as proposed in [13], or the power output can be reduced. If possible the LED must be positioned at the bottom to avoid increase in the retina's temperature.

The study establishes the power budget limit for the intraocular projector device to be approximately 100 mW. It provides important information on the power and heat budget for electronic intraocular devices. The prosthesis devices are currently under testing for vision restoration in blind eyes. In the future, such electronic intraocular implants have the potential for widespread adoption as vision augmentation devices.

Acknowledgment

This research is partially funded by US Department of Defense grant *VR180058* and US NIH National Eye Institute grant K08EY27469. This support is gratefully acknowledged.

Conflict of Interest

There are no conflicts of interest.

Data Availability Statement

Data are provided by a third party listed in Acknowledgment.

Nomenclature

c = specific heat capacity (J/Kg C)
k = thermal conductivity (W/mC)
t = time (s)
Q = metabolic heat generation (W/m^3)
T = temperature (°C)
c_b = specific heat capacity of blood (J/Kg C)
T_b = blood temperature (°C)
ρ = density (kg/m^3)
ρ_b = density of blood (kg/m^3)
ω_b = volumetric blood perfusion rate (1/s)

References

[1] Bartels, M., Doxiadis, I., Colen, T., and Beekhuis, W., 2003, "Long-Term Outcome in High-Risk Corneal Transplantation and the Influence of HLA-A and HLA-B Matching," Cornea, **22**(6), pp. 552–556.
[2] Gain, P., Jullienne, R., Aldossary, M., Acquart, S., Cognasse, F., and Thuret, G., 2016, "Global Survey of Corneal Transplantation and Eye Banking," JAMA Ophthalmol., **134**(2), pp. 167–173.
[3] Shim, S., Gong, S., Rosenblatt, M., Palanker, D., Al-Qahtani, A., Sun, M., Zhou, Q., Kanu, L., Chau, F., and Yu, C., 2019, "Feasibility of Intraocular Projection for Treatment of Intractable Corneal Opacity," Cornea, **38**(4), pp. 523–527.
[4] Shim, S., Gong, S., Fan, V., Rosenblatt, M., Al-Qahtani, A., Sun, M., Zhou, Q., Kanu, L., Vieira, I., and Yu, C., 2020, "Characterization of An Electronic Corneal Prosthesis System," Current Eye Res., **45**(8), pp. 1–7, PMID: 31886728.
[5] Lazzi, G., 2005, "Thermal Effects of Bioimplants," IEEE Eng. Med. Biology Magaz., **24**(5), pp. 75–81.
[6] Service, S. C., 2003. "ISO 14708-1: Implants for Surgery-Active Implantable Medical Devices—Part 1: General Requirements for Safety, Marking and for Information to be Provided by the Manufacturer." *Communication*.
[7] Piyathaisere, D., Margalit, E., Chen, S., Shyu, J., D'Anna, S., Weiland, J., Grebe, R., Grebe, L., Fujii, G., Kim, S., Greenberg, R., De Juan Jr, E., and Humayun, M., 2003, "Heat Effects on the Retina.," Ophthalmic Surg Lasers Imaging Retina, **34**(2), pp. 114–120.
[8] DeMarco, S., Lazzi, G., Wentai, L., Weiland, J., and Humayun, M., 2003, "Computed SAR and Thermal Elevation in a 0.25-mm 2-d Model of the Human Eye and Head in Response to An Implanted Retinal Stimulator - Part I: Models and Methods," IEEE Trans. Antennas Propagat., **51**(9), pp. 2274–2285.
[9] Gosalia, K., Weiland, J., Humayun, M., and Lazzi, G., 2004, "Thermal Elevation in the Human Eye and Head Due to the Operation of a Retinal Prosthesis," IEEE Trans. Biomed. Eng., **51**(8), pp. 1469–1477.
[10] Opie, N. L., Burkitt, A. N., Meffin, H., and Grayden, D. B., 2010, "Thermal Heating of a Retinal Prosthesis: Thermal Model and In-Vitro Study," 2010 Annual International Conference of the IEEE Engineering in Medicine and Biology, pp. 1597–1600.
[11] Opie, N. L., Burkitt, A. N., Meffin, H., and Grayden, D. B., 2012, "Heating of the Eye by a Retinal Prosthesis: Modeling, Cadaver and in Vivo Study," IEEE Trans. Biomed. Eng., **59**(2), pp. 339–345.
[12] Stark, J., Foster, C., and Yu, C., 2021, "Axisymmetric Thermal Finite Element Analysis of Effects of Intraocular Projector in the Human Eye," J. Undergraduate Res., **17**(4).
[13] Gongal, D., Thakur, S., Panse, A., Pawar, R., Foster, C., and Yu, C., 2020, "Thermal Analysis of Intraocular Electronic Display Projector Visual Prosthesis," Numer. Heat Trans., Part A: Appl., **78**(12), pp. 706–716.
[14] Gokul, K.C., Gurung, D. B., and Adhikary, P. R., 2014, "Modeling Airflow Effects in Human Eye Temperature With and Without Eyelids," Int. J. Appl. Math. Mech., **32**, pp. 649–663.
[15] Scott, J. A., 1988, "A Finite Element Model of Heat Transport in the Human Eye," Phys. Med. Biol., **33**(2), pp. 227–242.
[16] Joukar, A., Nammakie, E., and Niroomand-Oscuii, H., 2015, "A Comparative Study of Thermal Effects of 3 Types of Laser in Eye: 3D Simulation With Bioheat Equation," J. Thermal Biology, **49–50**, pp. 74–81.
[17] Narasimhan, A., Jha, K. K., and Gopal, L., 2010, "Transient Simulations of Heat Transfer in Human Eye Undergoing Laser Surgery," Int. J. Heat. Mass. Transfer., **53**(1–3), pp. 482–490.
[18] Wessapan, T., and Rattanadecho, P., 2015, "Heat Transfer Analysis of the Human Eye During Exposure to Sauna Therapy," Numer. Heat Trans., Part A: Appl., **68**(5), pp. 566–582.
[19] Narasimhan, A., and Sundarraj, C., 2013, "Effect of Choroidal Blood Perfusion and Natural Convection in Vitreous Humor During Transpupillary Thermotherapy (TTT)," Int. J. Numer. Method Biomed Eng., **29**(4), pp. 530–541.
[20] Ooi, E. H., and Ng, E. Y. K., 2008, "Simulation of Aqueous Humor Hydrodynamics in Human Eye Heat Transfer," Comput. Biology Med., **38**(2), pp. 252–262.
[21] Tiang, K. L., and Ooi, E. H., 2016, "Effects of Aqueous Humor Hydrodynamics on Human Eye Heat Transfer Under External Heat Sources," Med. Eng. Phys., **38**(8), pp. 776–784.
[22] Canning, C., Greaney, M., Dewynne, J., and Fitt, A., 2002, "Fluid Flow in the Anterior Chamber of a Human Eye," IMA J. Math. Appl. Med. Biology, **19**(1), pp. 31–60.
[23] Kumar, S., Acharya, S., Beuerman, R., and Palkama, A., 2006, "Numerical Solution of Ocular Fluid Dynamics in a Rabbit Eye: Parametric Effects," Ann. Biomed. Eng., **34**(3), pp. 530–544.
[24] Thompson, K., Bhardwaj, R., and Nguyen, T., 2017, "Development of an Anatomically Accurate Finite Element Human Ocular Globe Model for Blast-Related Fluid-Structure Interaction Studies. US Army Research Laboratory Report ARLTR-7945.
[25] Barajas, M. H., *Atlas of the Human Eye: Anatomy & Biometrics*, Palibrioy, Bloomington, IN.
[26] Li, Y., and Huang, D., 2009, "Pupil Size and Iris Thickness Difference Between Asians and Caucasians Measured by Optical Coherence Tomography," Invest. Ophthalmol. Visual. Sci., **50**(3), pp. 1552–5783.
[27] Lagendijk, J. J., 1982, "A Mathematical Model to Calculate Temperature Distributions in Human and Rabbit Eyes During Hyperthermic Treatment," Phys. Med. Biol., **27**(11), pp. 1301–1311.
[28] Scott, J. A., 1988, "The Computation of Temperature Rises in the Human Eye Induced by Infrared Radiation," Phys. Med. Biol., **33**(2), pp. 243–257.
[29] Flyckt, V. M., Raaymakers, B. W., and Lagendijk, J. J., 2006, "Modelling the Impact of Blood Flow on the Temperature Distribution in the Human Eye and the Orbit: Fixed Heat Transfer Coefficients Versus the Pennes Bioheat Model Versus Discrete Blood Vessels," Phys. Med. Biol., **51**(19), pp. 5007–5021.
[30] Ng, E., and Ooi, E., 2006, "FEM Simulation of the Eye Structure With Bioheat Analysis," Comput. Methods Programs Biomed., **82**(3), pp. 268–276.
[31] Shafahi, M., and Vafai, K., 2011, "Human Eye Response to Thermal Disturbances," ASME J. Heat. Transfer., **133**(1), p. 011009.
[32] Wessapan, T., and Rattanadecho, P., 2013, "Specific Absorption Rate and Temperature Increase in the Human Eye Due to Electromagnetic Fields Exposure At Different Frequencies," Int. J. Heat. Mass. Transfer., **64**, pp. 426–435.
[33] Nayar, K., Sharqawy, M., Banchik, L., and Lienhard V, J., 2016, "Thermophysical Properties of Seawater: A Review and New Correlations that Include Pressure Dependence," Desalination, **390**, pp. 1–24.
[34] Sharqawy, M. H., Lienhard V, J. H., and Zubair, S. M., 2010, "Thermophysical Properties of Seawater: A Review of Existing Correlations and Data," Desalin. Water. Treat., **16**(1–3), pp. 354–380.
[35] Ozbek, H., Fair, J. A., and Phillips, S. L., 1977, "Viscosity of Aqueous Sodium Chloride Solutions From 0 - 150o c".
[36] MIT.edu. 6.777j/2.751j Material properties database, http://mit.edu/~6.777/matprops/matprops.htm, Accessed March 29, 2020.
[37] Technologies, C.-T., The Thermal Conductivity of Unfilled Plastics, https://ctherm.com/resources/blog/the_thermal_conductivity_of_unfilled_plastics/, Accessed March 29, 2020.
[38] MatWeb, M. P. D. Overview of Materials for Epoxy Adhesive, http://www.matweb.com/search/datasheettext.aspx?matguid=c1ec1ad603c74f628578663aaf 44f261, Accessed March 29, 2020.
[39] Glass properties — Saint-Gobain Sekurit, https://www.saint-gobain-sekurit.com/glossary/glass-properties, Accessed March 28, 2020.